Draft version April 24, 2015
Preprint typeset using LaTeX style emulateapj v. 12/16/11

DETECTING ACTIVE ASTEROIDS/COMETS FROM OSSOS SURVEY IMAGES

Authors
Affiliations
Draft version April 24, 2015

ABSTRACT

Abstract.
Keywords: keywords

1. INTRODUCTION

Until the last decade [todo: WC?], comets and asteroids have been thought of as separate populations differing in both morphology and dynamics. With different fractions of volatile content, an obvious dintinction is the presence of a transient coma and/or tail around a comet, whereas asteroids exhibit bare nuclei photometric properties. [todo: mention Tisserand parameter here?] With the recent advent of large wide-field surveys which have regularly monitored large populations of solar system objects, objects which exist between the classification of comets and asteroids have begun to be identified. The classical view of comets being rocky ice bodies with highly eccentric orbits, and asteroids being icy rock bodies with stable orbits confined to the main asteroid belt between Mars and Jupiter (Sheppard and Trujillo 2015), has been usurped [todo: WC?] by the discovery of comet-asteroid transition objects. Asteroids in dynamically cometary orbits, dynamically asteroidal objects that exhibit burst of cometary activity or are associated with meteor streams such as the Damocloids (Sonnett et al. (2011); and references therein, Gilbert and Wiegert (2009)) exist between the accustomed classification criteria. These objects may be comets which have exhausted their volatile content or are dormant, or asteroids which have a higher volatile fraction. In this study we focus on the "active asteroids" (AAs) (or main belt comets (MBCs)), which are a population of bodies with stable asteroid-like main belt orbits that exhibit transient comae and/or tails consistent with cometary morphology. As it is expected that icy objects in the inner solar system would have long ago sublimated, the active asteroids pose an interesting insight to the heliocentric distance at which ice condenses, known as the 'snow line', which of interest to planetary formation and determining the chemistry of the early solar nebula.

For objects which formed in the the outer region of the main belt, the crystallized water ice which was present at the time of formation and not exposed to primordial heating may still remain in reservoirs beneath the surface (Prialnik and Rosenberg 2009). According to models developed by Fanale and Salvail (1989), beyond heliocentric distances of 2.4 AU ice can be protected against sublimation by a relatively thin surface regolith of depth 1 – 100 m for the entire age of the solar system. If the ice layer were to be exposed to sub solar heating by a triggering event, sublimation could eject dust particles from the surface. The source of the dust emission may be different for each object and could include ice sublimation, impact ejecta, rotational instabilities due to YORP torques, or a combination of several effects. (Hsieh et al. (2015); and references therein) [todo: include references here instead].

Since the first discovery of an active main-belt asteroid, 133P/Elst-Pizarro (Elst et al. 1996), several attempts have been made to identify new objects of this type; at present, eighteen objects have been identified with diverse orbital dynamics [todo: WC?] (Figure 1) [todo: check figure reference] (Jewitt et al. 2015). A comprehensive review of these surveys can be found in Hsieh et al. (2015). A persistent challenge to this effort is that the detection of the faint coma or tails around small dark objects is highly dependent on the magnitude constraints of the survey. As most asteroids fall near the limiting magnitude of the survey in which they are discovered [todo: citation necessary?], objects which are larger, closer, or have higher albedo are preferentially detected and any dust emission would be more easily apparent. At present, the active fraction of identified active asteroids greater than 1 km to main belt asteroids greater than 1 km is $f \sim 10^5$, and describes a strong lower limit as many objects are yet undetected. (Jewitt et al. 2015)

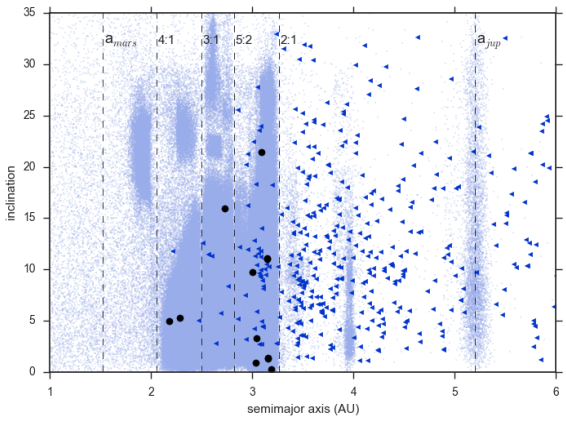

Figure 1. Inclination of all objects in the main asteroid belt from the AstDys catalogue as a function of semimajor axis. Mean motion resonances between Mars and Jupiter as well as the planet's semimajor axis are marked in dashed lines, main belt objects are marked as light small dots, comets as arrows, and active asteroids as stars.

In this paper, we present a study of main belt objects present in the Canada-France-Hawaii Telescope (CFHT) Outer Solar System Origins Survey (OSSOS) data to identify the presence of cometary-like activity. Pre-

viously undetectable emission activity may be able to be identified in the OSSOS survey, which has a limiting magnitude much lower than previous surveys (Hsieh et al. 2015) [todo: check that magnitudes listed in this paper]. We select the Hungaria family as the test group for our search pipeline. Potential activity is identified by measuring the asteroids brightness profile and comparing this to a stellar model profile of the same magnitude in order to detect a large deviation in width potentially characteristic of a coma or jet. Asteroids which have residuals larger than a 3 sigma deviation are subjected to visual examination. This is similar to the process employed by Luu (1992), Sonnett et al. (2011), and Gilbert and Wiegert (2009). [todo: Include Lixiaohua family]

2. OBSERVATIONS

Observations taken by OSSOS with the CFHT MegaPrime wide-field optical imaging facility at the summit of Mauna Kea, Hawaii, have been collected since February 2013. The wide-field imager MegaCam is a 36 CCD image plane, each 2048 x 4125 CCD with resolution of 0.185"/pix. This covers a field of $\sim 1^\circ$ x 1° on the sky. Each block of data taken consists of a mosaic of 21 segments of one-square-degree sky coverage, and at present, covers two orbital phase spaces on the plane of the ecliptic, and two off plane at low inclinations. The OSSOS survey employs the u* and r' filters on the MegaCam with integration times of 287, 387, and 500 seconds, yielding a lower limit of $m_r \sim 24.5$ magnitudes.

The OSSOS images were pre-processed by standard data detrending with the MegaPipe image stacking pipeline [todo: check if this is correct]. An astrometric correction was applied by [todo: sgwyn, check if there is a reference]. Source characteristic measurements were obtained from Source Extraction and Photometry in Python (SEP) and were used to extract the orbital information the transient objects.

The survey covers a wide field of both the ecliptic plane and low inclinations allowing for the observation of a large number of main belt objects in different orbital phase spaces. This can be seen in Figure 2. As the observations were not targeted to specific main-belt populations, the survey is relatively unbiased, and we can put constraints on the number of AAs in the whole of the main asteroid belt.

3. ANALYSIS

From the calculated arcs provided by the Solar System Object Image Search (SSOIS) ephemeris (Gwyn et al. 2012) of 671,234 main belt objects in the Asteroids Dynamic Site (AstDys) catalogue (AstDys 2015) we were able to predict which asteroids were present in the OSSOS data set and could be examined for cometary activity. From a set of 3,528 images, there are 201,477 observations of 46,367 objects in the OSSOS data. We analyze a small group of objects in the Hungaria family as our test case for our automated pipeline. Of the 1187 Hungarias we have 76 observations of 25 objects.

We use a two-step pipeline to first identify the precise coordinates of each asteroid, and measure the brightness profile of the point spread function (PSF). The profiles are then compared to stellar models for significant deviations. [todo: change this sentence]

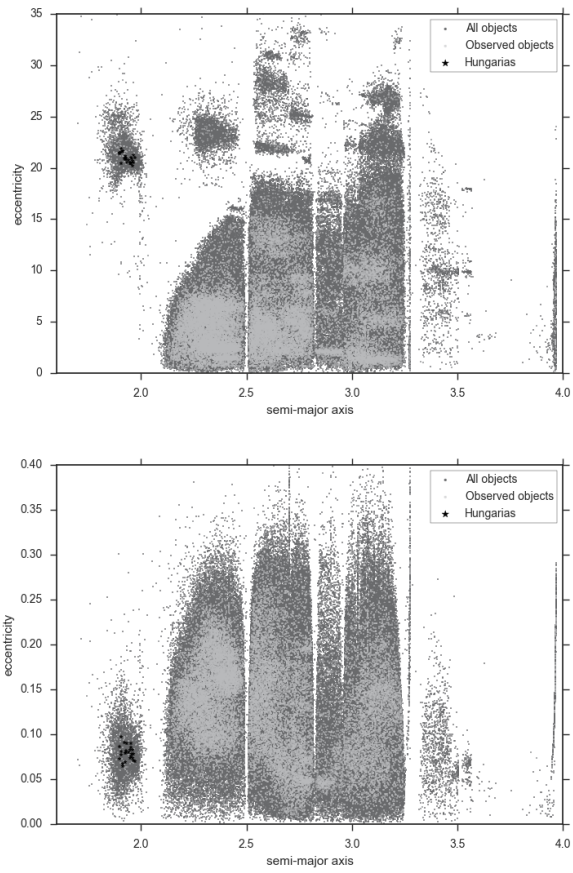

Figure 2. The inclination and eccentricity as a function of semi-major axis of all known objects in the main asteroid belt, objects observed by OSSOS, and the Hungaria family test group.

Figure 3. The number of observations by OSSOS of each asteroid.

3.1. *Object identification*

An automated pipeline was written to identify each asteroid in an OSSOS exposure by: location relative to the predicted coordinates, elongation due to trailing effects caused by the apparent rate of motion over the duration

of the exposure, and apparent magnitude.

The coordinates of each object in the exposure were obtained from the photometric software SEP, and objects which were closest to the predicted location (at the midpoint of the exposure) as calculated by known arc (JPL 2015) [todo: is this citation necessary?] were chosen as candidate objects. If no objects were detected within a set radius calculated from the uncertainty in the asteroid arc, the radius was increased by a factor of 1.5 and the search was repeated.

The predicted elongation of the trail was calculated from the motion of the asteroid over the length of the exposure (JPL 2015) under the assumption of constant motion. This was compared to the elliptical shape parameters measured by SEP for each candidate object. A difficulty in this process is that objects which move faster during the exposure, and thus have longer trails, will be less elliptical in shape. As the photometry software is optimized for point sources and extended sources such as galaxies, the accuracy of the shape parameters to be correlated to the extent of the elongation. For this reason we implement an uncertainty of 20 percent on the elongation measure, with the expectation that only objects which are markably inconsistent would be rejected. For greatly extended trails, with a ratio of semi-major axis to semi-minor axis of 5:1, SEP incorrectly resolves the asteroid as two separate objects as the flux spread was not necessarily constant over the length. An example of such an object is shown in Figure 2 [todo: fig ref]. In this case both objects would meet the location and magnitude conditions, pass through the same consistency level, and be flagged for visual inspection.

The inability of the photometry software to correctly measure the shape of the asteroid trail would also have an affect on the measured flux as the aperture may not include the total amount of light. As the centre of the object is determined by the flux weighted barycenter of the object, this may also result in an inaccurate measurement of the astrometry. In order to avoid this error, the centre coordinates of the object were chosen as the centre of the elliptical aperture for fast-moving objects. In addition, the elongation effect in itself may affect the accuracy of the flux measurement without taking into account the potential loss of light. This is a result of the flux being spread over a larger area than the point spread function (PSF), which reduces the per unit area apparent magnitude and the signal-to-noise (Vereš et al. 2012). A direct consequence is a lowered limiting magnitude for fast moving asteroids. A third consideration is that objects which are active and have jets or a coma will appear brighter than the expected magnitude calculated from previous observations. Depending on the extent of the activity, this could cause the object to be measured as several magnitudes greater than predicted. For these reasons, in subjecting the candidate object to a consistency check with the predicted value we used an uncertainty of 2 magnitudes (unless the object was predicted to vary by a larger amount in the span of 10 days following the exposure) and did not reject the object if it was inconsistent.

In order to accurately measure the PSF of the asteroid – which is necessary to check for anomalous flux surrounding the object that could indicate activity – it is necessary to ensure that the asteroid is isolated from other sources. A catalogue of bright sources [todo: cite Cwynn?]was built for the OSSOS data set from a collection of exposures with excellent photometry, and was used to ensure that the asteroids were not involved with a background source.

A candidate object which did not meet any of the criteria mentioned above would be rejected. Objects which met the location and elongation conditions were preferentially selected over those that only met the location and magnitude conditions. If multiple objects met the same level of criteria, they would be rejected and followed up with visual inspection.

Applying this identification process left 66 exposures of 21 asteroids to be examined.

Table 1
Rejection cause for images through identification pipeline

Total number of images	76
Rejection cause	**# images**
Involved with background stars	1
Off the edge of the CCD	5
In saturated region of nearby bright star	1
In diffraction region of nearby bright star	1
Bad exposure	4
Retained	64

3.2. *Rejection causes*

Involved: When compared with a catalogue of bright sources [todo: cite Gwyn?] the object was found to spatially coincide with a background object. As the catalogue was built from a set of exposures with good photometry, asteroids present in those exposures would be incorrectly identified as involved. [todo: can we get a list of the exposures used?] Not included in the catalogue are dim sources, transient objects, and bad pixels/columns. In the case of the asteroid being involved with such objects, the photometry software would measure the convolved sources, and the elongation and magnitude would be inconsistent with the predicted values. If the background object were dim enough that the convolved source passed the magnitude condition, the PSF would be beyond the 5 sigma deviation, and the involvement would be caught by visual inspection. An example of such a case is shown in Figure 2 [todo: reference figure].

Not on the CCD: If the SSOIS query incorrectly identified that an asteroid was on in an OSSOS exposure, but rather the object was within a few degrees off the edge of the CCD, no object would be found in the uncertainty ellipse of the predicted location.

In saturated region of a nearby bright source: For object close to, but not involved with, bright sources the asteroid may in the diffraction region of the saturated pixels. In this case no object would be found in the uncertainty ellipse around the predicted co-ordinates.

Bad exposure: Exposures which were marked as bad were automatically rejected. This would include tracking errors, short exposures, poor image quality, and corrupted images.

3.3. *PSF comparison*

A postage stamp of size 2.5 times the full-width-half-maximum (FWHM) and centred on the midpoint of the elongated shape was rotated such that asteroid trail was aligned parallel to the pixel rows on the CCD chip. The asteroid profile was averaged over the entire length of the postage stamp. The stellar model PSF was built from the OSSOS MOP at the location of and with the same magnitude as the asteroid on the CCD to account for any distortion, and rotated by the same angle. The profile was measured as the average over the width of the model star. A 3 sigma difference between the subtracted profiles was used to indicate the presence of additional flux around an asteroid, characteristic of a cometary comae. There were [fill in] asteroids which were measured to be above this limit and were flagged for visual confirmation. Due to saturation effects, asteroids with magnitudes greater than 18.5 were not analyzed for activity. However, as previous surveys have included this set of objects (Hsieh et al. 2015) we were comfortable with this exclusion.

3.4. *Detection Efficiency*

How well do we identify coma vs jets vs tails ? How may do we detect vs observed? What are the statistics? Why are the results so bad?

4. DISCUSSION

4.1. *Identification criteria*

The given uncertainty of 20 percent was found to be a robust [todo: WC?] as the percent difference between the predicted and measured elongations for all objects correctly measured by SEP was under 18 percent, and with a mean of 8 percent. This was therefore a good value for only rejecting objects which were not the intended asteroid or not properly measured.

Despite the expectation that the elongation would be correlated to the inaccurate measurement of the magnitude due to the spread of the flux, no statistical relationship was found between the difference of the predicted and measured magnitude and the elongation.

4.2. *Photometry errors*

All objects which were successfully identified passed the elongation condition How many objects were 'very' elongated?

As the involvement test was preformed from a catalogue of bright objects, it is possible that asteroids involved with dim background objects were not properly flagged. An example of this is shown in Figure 4. Depending on the geometry of the involvement this could be selected as an asteroid with activity, possibly with a large bright jet. The involvement would then be determined in the visual examination of all asteroids with brightness profiles with larger than a 3 sigma deviation from the background residuals [todo: WC?]. An obvious distinction between a background source and a jet is that the outflow would be trailed to the same extent of the asteroid.

5. RECOMMENDATIONS

Use a trail fitting function for improved photometry on fast moving objects such as described by Vereš et al. (2012). Tail detection pipeline like Sonnett et al. (2011)

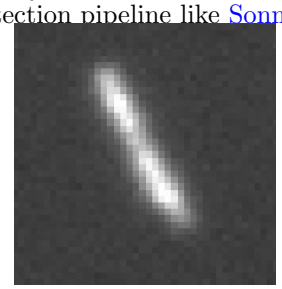

Figure 4. A Fast moving asteroid trailed over the duration of the exposure with an uneven flux spread over its length. This object required visual inspection as it was incorrectly resolved as multiple objects by SEP

Acknowledgments.

REFERENCES

AstDys, 2015. URL http://hamilton.dm.unipi.it/astdys/index.php?pc=5.

Kyle Barbary and contributors, 2015. URL http://sep.readthedocs.org/en/v0.3.x/.

E. W. Elst, O. Pizarro, C. Pollas, J. Ticha, M. Tichy, Z. Moravec, W. Offutt, and B. G. Marsden. Comet P/1996 N2 (Elst-Pizarro). IAU Circ., 6456:1, aug 1996.

F. P. Fanale and J. R. Salvail. The water regime of asteroid (1) Ceres. Icarus, 82:97–110, nov 1989. doi:10.1016/0019-1035(89)90026-2.

A. M. Gilbert and P. A. Wiegert. Searching for main-belt comets using the Canada-France-Hawaii Telescope Legacy Survey. Icarus, 201:714–718, jun 2009. doi:10.1016/j.icarus.2009.01.011.

S. D. J. Gwyn, N. Hill, and J. J. Kavelaars. SSOS: A Moving-Object Image Search Tool for Asteroid Precovery. PASP, 124:579–585, jun 2012. doi:10.1086/666462.

H. H. Hsieh, L. Denneau, R. J. Wainscoat, N. Schörghofer, B. Bolin, A. Fitzsimmons, R. Jedicke, J. Kleyna, M. Micheli, P. Vereš, N. Kaiser, K. C. Chambers, W. S. Burgett, H. Flewelling, K. W. Hodapp, E. A. Magnier, J. S. Morgan, P. A. Price, J. L. Tonry, and C. Waters. The main-belt comets: The Pan-STARRS1 perspective. Icarus, 248:289–312, mar 2015. doi:10.1016/j.icarus.2014.10.031.

D. Jewitt, H. Hsieh, and J. Agarwal. The Active Asteroids. *ArXiv e-prints*, feb 2015.

JPL, 2015. URL http://hamilton.dm.unipi.it/astdys/index.php?pc=5.

J. X. Luu. High resolution surface brightness profiles of near-earth asteroids. Icarus, 97:276–287, jun 1992. doi:10.1016/0019-1035(92)90134-S.

D. Prialnik and E. D. Rosenberg. Can ice survive in main-belt comets? Long-term evolution models of comet 133P/Elst-Pizarro. MNRAS, 399:L79–L83, oct 2009. doi:10.1111/j.1745-3933.2009.00727.x.

S. S. Sheppard and C. Trujillo. Discovery and Characteristics of the Rapidly Rotating Active Asteroid (62412) 2000 SY178 in the Main Belt. AJ, 149:44, feb 2015. doi:10.1088/0004-6256/149/2/44.

S. Sonnett, J. Kleyna, R. Jedicke, and J. Masiero. Limits on the size and orbit distribution of main belt comets. Icarus, 215: 534–546, oct 2011. doi:10.1016/j.icarus.2011.08.001.

The International Astonomical Union, 2015. URL http://www.minorplanetcenter.net/iau/MPCORB.html.

P. Vereš, R. Jedicke, L. Denneau, R. Wainscoat, M. J. Holman, and H.-W. Lin. Improved Asteroid Astrometry and Photometry with Trail Fitting. PASP, 124:1197–1207, nov 2012. doi:10.1086/668616.

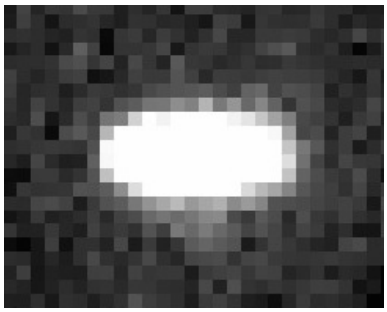

Figure 5. An asteroid involved with a dim background object.